Aerodynamic Loading on Crew Access Arm

T.J. Wignall,* Jesse Collins,† and Brent Pomeroy.‡
NASA Langley Research Center, Hampton, VA 23681

To help ensure the Crew Access Arm (CAA) used with the NASA Space Launch System (SLS) met desired performance, an aerodynamic database for the CAA during deployment is generated. While initial attempts used data derived from wind tunnel testing, limitations in hardware led to the use of computational fluid dynamics to gather data at conditions not achievable in the wind tunnel. This computational data compared favorably to the experimental data increasing confidence in both. Further analysis led to simplification showing the ability to build the database with a single relative wind variable, which takes into account both arm deployment angle and wind direction. Both geometric and computational simplifications, such as a simplified tower and a stationary CAA, were made such that the simulations could be executed with reasonable fidelity without excessive computational cost. These static conditions are then compared to a dynamic simulation where the CAA rotates into position to test the quasisteady state assumptions used to generate the database. The dynamic case showed an increase in the moment about the CAA hinge but within the uncertainty bounds delivered with the database.

I. Nomenclature

CAA	=	Crew Access Arm
CFD	=	Computational Fluid Dynamics
ML	=	Mobile Launcher
SLS	=	Space Launch System
WT	=	Wind Tunnel
$\hat{C}_Y$	=	Normalized side force coefficient
$\hat{C}_{m,hinge}$	=	Normalized moment about the x-axis at the CAA hinge
ϕ_{azm}	=	Wind Angle (deg)
γ	=	CAA deployment angle (deg)
Θ	=	Relative Wing Angle (deg)

II. Introduction

The crew access arm (CAA) is used to allow people to access crewed spacecraft for boarding and final systems checks before launch. While many launch vehicles use a similar setup, the CAA of interest is designed and operated by NASA's Exploration Ground Systems and takes astronauts from the Mobile Launcher (ML) to the Orion spacecraft sitting atop the Space Launch System (SLS). Operation of the CAA, especially during emergency egress, relies on proper characterization of the aerodynamic environment. As part of the Artemis Program's goal to return astronauts to the moon, ensuring safe operations of these systems is a priority. Recent work constructed an aerodynamic database to characterize the ground wind loads on the CAA to ensure safety critical operations can be met.

The initial data gathered for this analysis were an additional, late requirement added to an ongoing effort to collect liftoff and transition flight phase data for both the WT and the CFD. The WT testing focused primarily on the loads across the whole ML and was not originally trying to characterize forces and moments on the umbilicals and arms. The initial CFD results come from simulations used to characterize the ground wind loads on the launch abort system hatch as it opened in case of emergency egress. As a consequence of originally being a secondary objective, some geometry simplifications were made that would likely not have been if CAA loads were the primary goal.

*Research Aerospace Engineer, Configuration Aerodynamics Branch, thomas.j.wignall@nasa.gov.
†Research Aerospace Engineer, Configuration Aerodynamics Branch, AIAA Member,
‡Research Aerospace Engineer, Configuration Aerodynamics Branch, AIAA Senior Member.

A. SLS/Artemis

While the SLS refers to a class of launch vehicles that come in both cargo and crew variants, the work here is relevant primarily to the crewed configurations, which have the Orion spacecraft as their payload. The prelaunch aerodynamic environment is defined primarily by the wind direction, ϕ_{azm}, which is defined as 0° from the North (ML side) and increasing clockwise so that winds from the East means ϕ_{azm} = 90°, which can be seen in Fig. 1a.

The aerodynamic database is designed specifically for the ML-1 and the Block 1 Crew as it is the planned configuration for the first crewed flight of the SLS. While design differences between ML-1 and ML-2 are significant in some areas, the CAA remains relatively unchanged. The largest difference is the increased height of the CAA on the ML-2 to account for the taller Block 1B Crew vehicle, as such the WT data are generated from a ML-2 configuration.

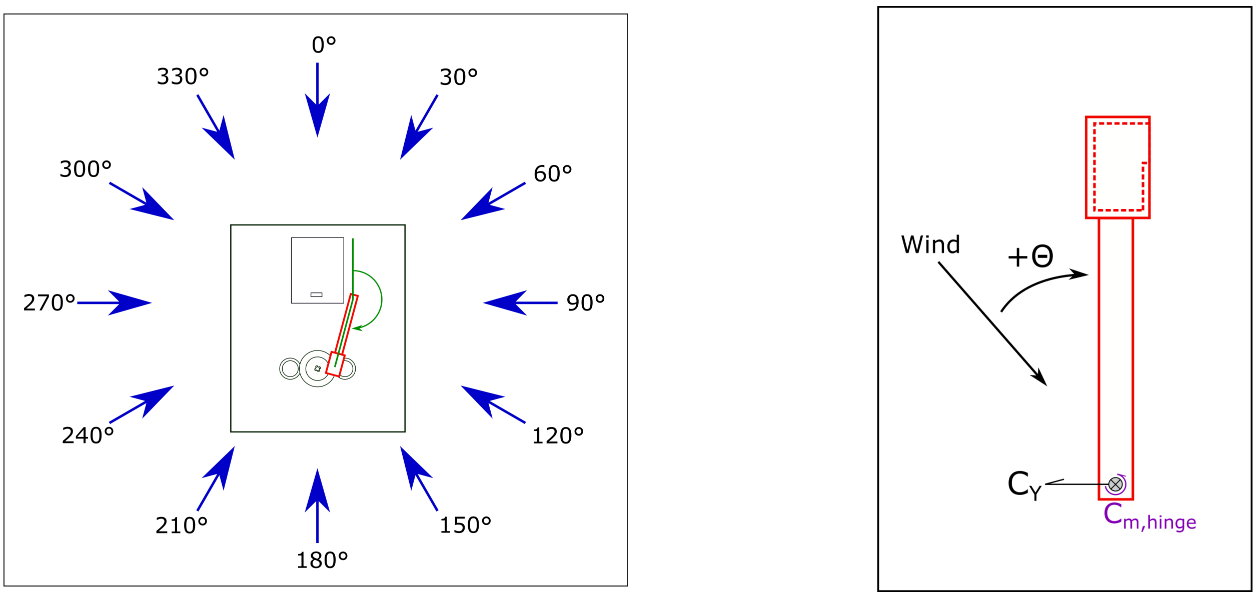

(a) ϕ_{azm} (blue) and γ (green)

(b) Θ, $\hat{C}_Y$ and $\hat{C}_{m,hinge}$

Fig. 1 Sketches of the primary variables of interest. (a) Wind azimuth (ϕ_{azm}) with blue arrows and deployment angle(γ) in green in relation to ML, vehicle, and CAA. (b) Relative wind (Θ), normalized side force coefficient ($\hat{C}_Y$), and normalized moment coefficient about the CAA hinge ($\hat{C}_{m,hinge}$).

B. Crew Access Arm

The CAA spans from the ML to the vehicle allowing for astronauts to enter the Orion spacecraft atop the SLS [1]. It is comprised of a catwalk that is open to the elements, which leads from the tower to the white room. During prelaunch activities, the white room is pressurized such that it acts like a clean room. Below the white room is another walkway allowing access to the service module of the Orion spacecraft. Located about 270 feet above the ML platform, the 60 foot long arm is hydraulically controlled. The deployment angle, γ, goes from 0°, which is the fully retracted position adjacent to the ML (as seen in Fig. 2a), to 195°, which is the fully deployed position adjacent to the vehicle (as seen in Fig. 2b). Partial deployment can be seen in Fig. 2c.

After the crew has boarded and approximately an hour before flight, the CAA is retracted; however, if there is an emergency requiring crew evacuation, the CAA must return to its fully deployed position in approximately 45 seconds. This design requirement necessitates computational simulations to determine the aerodynamic loading on the structure. An aerodynamic database characterizing the loading from ground winds on the CAA was constructed. Only the forces and moments that contribute to the rotation of interest are tracked, in this case normalized side force coefficient, $\hat{C}_Y$, and the normalized moment about the x-axis at the CAA hinge, $\hat{C}_{m,hinge}$. The side force ($\hat{C}_Y$) is a body centered force and so rotates with the CAA as it rotates through its deployment. While $\hat{C}_{m,hinge}$ fully encompasses the effects of $\hat{C}_Y$, by providing both, the database user may move the center of rotation if needed. Because of export restrictions on the data, the results presented in this paper are normalized so that all values fall between -1 and 1, which is represented by the caret above the C. To look at it a different way, results are presented as a percent of the maximum loading.

The original plan was to deliver these aerodynamic coefficients as a function of ϕ_{azm} and γ; however, during analysis it was determined that a single variable was sufficient. The ϕ_{azm} and γ were able to be combined into a relative wind angle, Θ, which was sufficient to characterize the coefficients of interest and is defined by

$$\Theta = \gamma - \phi_{azm}. \tag{1}$$

A sketch of these definitions along with $\hat{C}_Y$ and $\hat{C}_{m,hinge}$ are found in Fig. 1b. Note that the definition of Θ is such that when the wind is blowing on the narrow end of the white room it is 0°. During analysis with this database, ϕ_{azm} will be considered constant and so this definition means that Θ will linearly increase as the CAA deploys.

(a) ML with CAA retracted

(b) Fully deployed CAA

(c) Partially deployed CAA

Fig. 2 Pictures of the CAA at various deployment angles. (a) Top of the ML with the CAA fully retracted [NASA/Jamie Peer], (b) the fully deployed CAA connecting the ML with Artemis 1 [NASA/Ben Smegelsky], (c) the CAA partially deployed [NASA/Kim Shiflett].

III. Wind Tunnel Experiment Setup

In the summer of 2021, a wind tunnel test was conducted at the NASA LaRC 14- by 22-Foot Subsonic Tunnel. This experiment investigated the liftoff and transition flight phases of the the NASA Block 1B launch vehicles. The descriptions herein refer to the liftoff phase of testing.

During this experiment, a novel measurement technique was employed to measure the load distribution on the ML, which is detailed in Ref. [2]. In this experiment, the SLS Block 1B vehicles and ML-2 were represented at 1.75% of full-scale size. Input flow conditions were a spatially uniform freestream of dynamic pressure equal to 50 psf. Individually metric load cells were distributed along the length of a centrally running support bar in the representative place of the full-scale ML-2 elevator shaft. Using 3D printing techniques, high geometric fidelity "tiers" were designed and constructed. These tiers are constructed as groups of floors that comprise the entire ML, and are mounted along the length of the support bar. As each tier is individually metric, slight gaps are included in the design that allow each metric piece of the assembly to exist and provide readings without fouling on one another.

The top-most tier in the design has a similar high-fidelity 3D printed representation of the CAA on it. Some geometric simplifications were made in order to allow for the part to be 3D printed. During testing, this CAA was able to be manually adjusted to one of two positions: fully retracted (γ = 0°) or fully deployed (γ = 195°). It can be seen in Figure 3 that the 3D printed version of the CAA accurately represents many important features of the full-scale CAA. Truss work features, the open catwalk, the open white room and weather seal (in the open position) are all built into the model-scale CAA. It could also be completely removed allowing the use of superposition assumptions to get a measurement of the loads on the CAA.

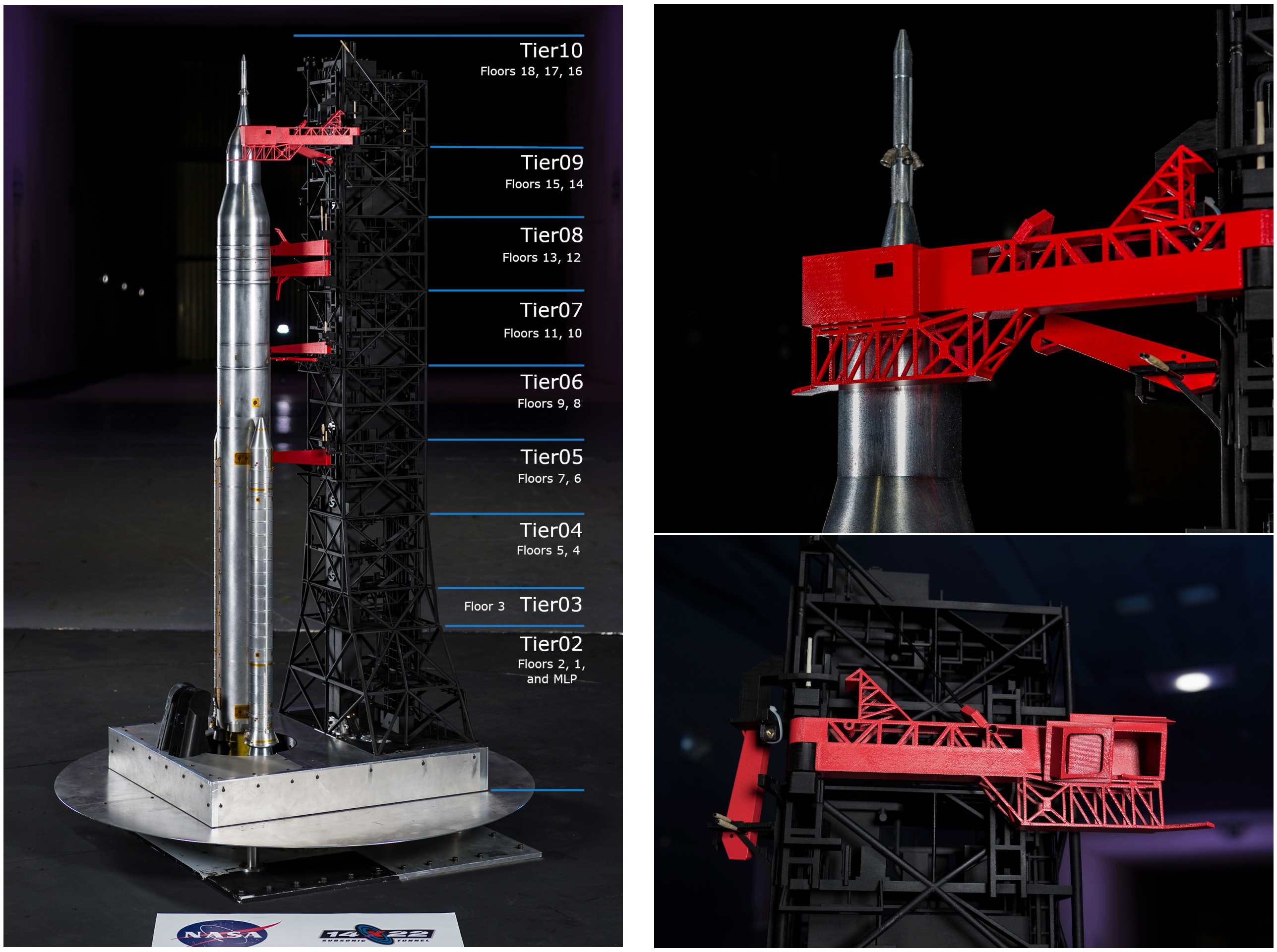

Fig. 3 Views of the entire ML-2 utilized in wind tunnel testing as well as the CAA in deployed (top right) and retracted (bottom right) positions.

A. Superposition Details

Due to the isolated and closely located individual tier balance to the CAA, a simple superposition method was utilized to estimate loads on the CAA alone. The basics of the superposition methods take measurements from the top tier load cell with the CAA attached and fully deployed, and compares them to measurements of the top tier load cell with the CAA removed. The logic is exemplified in Fig. 4. In the subfigures of Fig. 4, the green dashed rectangle represents the force and moment measuring device specific to Tier10 (on which the CAA is anchored). The scenario in Fig. 4a shows a WT measured run where: individually metric Tier10 records body-axis forces and moments as a function of ϕ_{azm}, the vehicle is present, all umbilical systems are deployed, and the CAA is present. The scenario in Fig. 4b shows a mostly similar second WT measured run where: individually metric Tier10 records body-axis forces and moments as a function of ϕ_{azm}, the vehicle is present, all umbilical systems are deployed, however, the CAA is removed from the test setup. The scenario in Fig. 4c then shows the desired result (via superposition) that if the previous 2 scenarios are subtracted from one another, the resulting forces and moments from that calculation should be attributable to the effects of the CAA for those test conditions (where the only difference between the two measured runs was the presence of the CAA). The results of this calculation are showed as the data series label “WT” on Figure 8 and are discussed further in Section V.A.

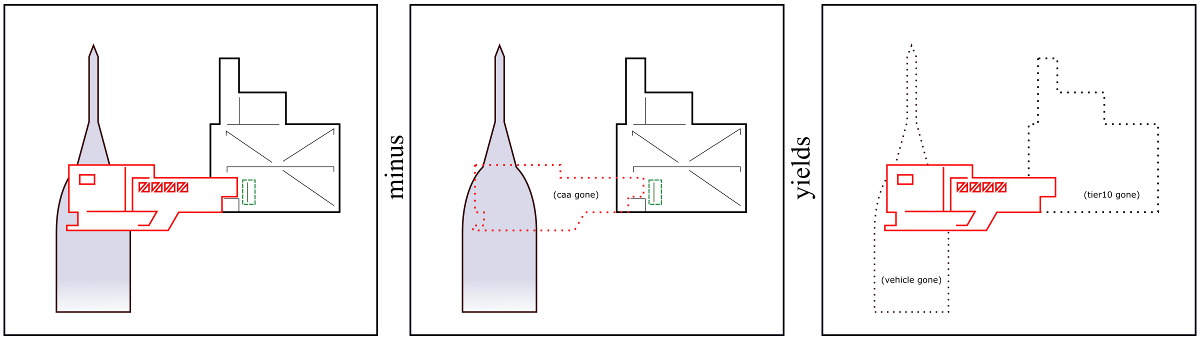

(a) Vehicle, ML, and CAA **(b) CAA removed** **(c) CAA only**

Fig. 4 Superposition of forces and moments demonstrated.

This methodology assumes the interaction between the different components has little effect on the net loading. With the CAA being in such close proximity to the vehicle, interactions with it were not considered in this calculation and without extra measurements would be difficult to quantify. A further assumption is that the differences between the ML-2 with the Block 1B crew and the ML-1 with the Block 1 crew is minimal. These limitations of superposition along with the inability to set the CAA at different γ values led to the use of CFD to help improve our predictions of CAA loading.

IV. Computational setup

Building off work done to help analyze aerodynamic loading on the Launch Abort System (LAS) hatch, the computational setup remains close to our baseline setup as laid out in Ref. [3]. Computational data were generated using the CREATE-AV Kestrel fluid dynamic solver [4–7]. It is a finite volume, cell centered unstructured grid solver that can be coupled with an off-body Cartesian grid solver (SAMAir), which can be executed with a static baseline Cartesian grid or with adaptive mesh refinement. Complex simulations, such as those in discussion, require significant computational resources, thus requiring off-body grid refinement for reasonable analysis. The flow is treated as fully turbulent and a Spalart-Allmaras turbulence model with Improved Delayed Detached Eddy Simulation is used. While solved time accurately, the data used in this analysis are time averaged over several thousand time steps except for the dynamic CAA case, which has no time averaging. Generally 10,000 time steps are used to allow transients to disperse and allow the flow to reach a statistically steady state before time averaging is done over 4,000 time steps. Simulations were performed with a dimensional time step of 0.0005 sec, corresponding to a nondimensional time step (dt*) of

$$dt^* = \frac{V_\infty}{D_{core}} dt \approx 0.004. \tag{2}$$

Freestream conditions were picked to match wind tunnel conditions. For more details on how the SLS program has used Kestrel for low speed aerodynamics see Refs. [3, 8–10].

Initial simulations used in this analysis were originally executed to support the LAS hatch loading work, and many decisions made for that work are carried over here [3]. As a result, the geometric simplifications to the CAA focused on balancing ease of calculation while maintaining enough fidelity to model the LAS hatch within the white room. Initial analysis, which included a simplified mobile launcher and vehicle, compared these LAS hatch runs to WT derived forces and moments as outlined in Section V.A. Building off these initial runs, various CAA deployment angles were simulated at critical wind directions. Due to computational cost of these runs and the criticality of the desired data, a CAA alone setup was developed and executed in parallel. These isolated CAA runs compared favorably to the higher fidelity solutions, and thus, CAA alone cases became the basis of the resulting aerodynamic database. Finally, since the resulting database is designed to be used with a moving body, a dynamic simulation was run with the CAA alone

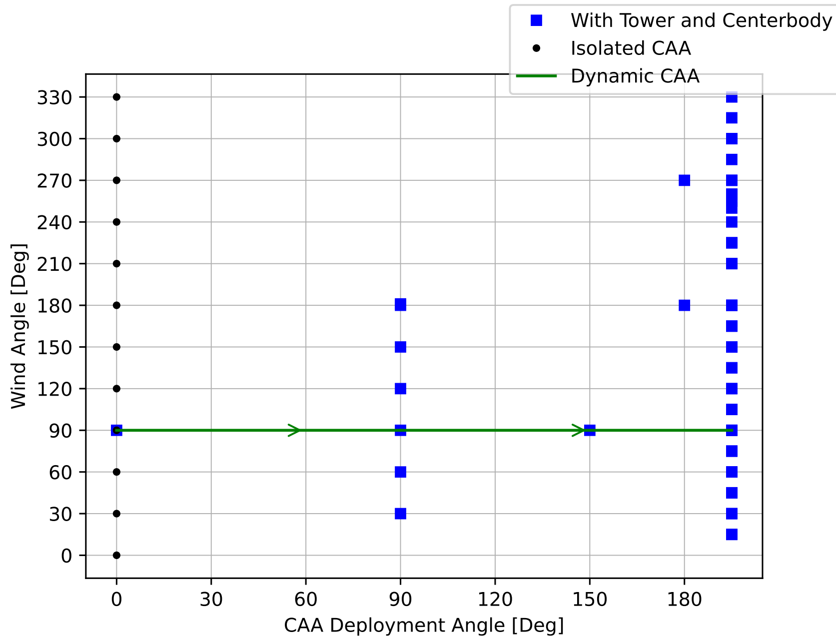

Fig. 5 Run matrix of the computational data. The arrows on the green line indicate direction of CAA movement.

rotating through space. The final run matrix is found in Fig. 5, which shows the tower and vehicle cases in blue squares, the isolated CAA as black circles and the dynamic CAA case as a green line.

A. CAA With Tower And Vehicle

Initial simulations were developed as a modification of the analysis done in support of the LAS hatch and when needed the refinement region was adjusted to focus on the CAA as opposed to the LAS hatch. As a result, all CFD data presented in this paper of the fully deployed CAA are from this initial exploration of aerodynamic loading on the LAS hatch, which also means that there are several data points for when the CAA is fully deployed.

The computational setup was simplified by the removal of geometric details from the simulated CAA and other modeled surfaces can be found in Fig. 6. The Mobile Launcher, based upon a simplified ML-1 geometry, is truncated about halfway down the structure wherein the truss structure is omitted while retaining the elevator shaft. The vehicle (in this case the Block 1 Crew) is simplified by removing the solid rocket boosters and other small geometric protuberances. Even with these geometric simplifications, about 100,000 processor hours across two days were needed for each simulation with some variation depending on γ and ϕ_{azm}.

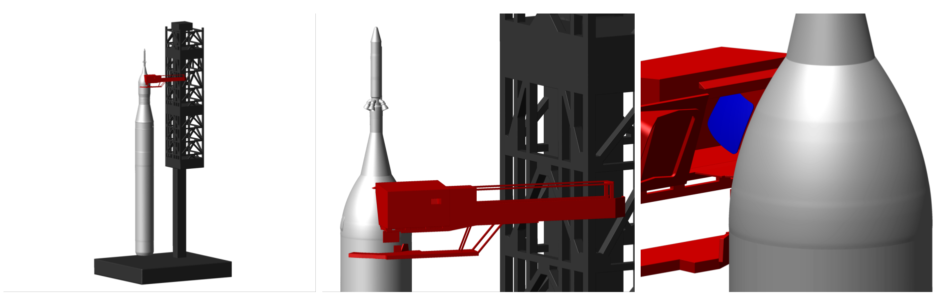

Fig. 6 Geometry used in simulations when ML and vehicle are present. The simplified ML in black, the simplified Block 1 Crew in grey, the CAA in red and the LAS hatch in blue. Some fully deployed CFD cases include the LAS hatch.

B. Isolated CAA

Simulations with the CAA are set up with the CAA fully retracted, which means that the $\Theta = -\phi_{azm}$. The same computational methods were employed for the CAA only simulations as the full-configuration simulations. These simulations showed transients clearing and the flow reaching a statistically-steady state much earlier than the full simulations; however, the same startup and time averaging setups were still used for consistency. Simulations were run every 30° to provided sufficient coverage of the parameter space. A more detailed picture of the simulated geometry is in Fig. 7. These simulations were much cheaper being approximately 12,000 processor hours and could have been further reduced if new time-averaging criteria were developed and used.

Fig. 7 Geometry of the CAA alone from two angles.

C. Dynamic Simulation

To ensure the validity of the quasisteady computational approach, a moving-body case was also run. The dynamic simulation was based on the CAA alone simulation; however, after reaching a statistically-steady state, the CAA was rotated 195° across approximately 17 seconds of simulation time. This 17 seconds was scaled from the real world value of 45 seconds based on the ratio of expected wind velocity on the pad to simulation velocity. To help reduce the number of required resources, the time step was increased from 0.0005 to 0.00075 sec. The refinement box of the CAA was set to follow the CAA as it moved. This single simulation took about 55,600 processor hours.

V. Analysis and Results

As discussed earlier, the driving motivation for this work was the development of an aerodynamic database that could be used in analysis to ensure that the CAA could get into position within a certain time frame. This section is organized in a similar matter to the data exploration that was undertaken during development of this aerodynamic database. First, the results from the wind tunnel are compared to the CFD at similar conditions. The limitations of the wind tunnel data to capture data at points where the CAA is not fully deployed led to exploration of using CFD to create the database. After favorable comparisons, it was decided to focus on using CFD to build the database. The computational cost and large parameter space turned our attention to running cases of the CAA alone to help narrow the run matrix. Results from the CAA alone compared favorably to the simulations with the tower and vehicle, which led to its use as the baseline of databases after the introduction of Θ. Finally, a case with the CAA moving was simulated to check the validity of quasisteady state assumptions used to build the database.

As mentioned earlier, since this paper uses data under export restrictions, which prevents the use of absolute scales, the forces and moments are normalized so that the values plotted fall between -1 and 1.

A. Fully Deployed CAA: WT to CFD

The first comparison is done by taking the wind tunnel derived side force and hinge moment coefficient from the wind tunnel and comparing them to the CFD of the fully deployed cases. These cases were originally part of the LAS hatch analysis, and thus, multiple solutions exist for each hatch deployment angle. These CFD data were generated using the simplified tower and vehicle. Comparisons of $\hat{C}_Y$ and $\hat{C}_{m,hinge}$ for these two datasets can be found in Fig 8. The black circles represent the force and moment coefficients calculated through superposition from the wind tunnel test data while the pink triangles are values from the CFD.

Despite the limitations in both datasets, excellent agreement is found between the computational and experimental data. While differences are expected due to the differences in the wind tunnel and CFD geometries, the agreement between the cases is encouraging. Both datasets capture similar peak structures at $\Theta = 90°$ and 270° with a slight difference in magnitude. The data capture a slight leveling out at $\Theta = 180°$ to 210° in both $\hat{C}_Y$ and $\hat{C}_{m,hinge}$, which is due to the ML being between the CAA and freestream flow. The one limitation to this dataset is that it only accounts for the CAA when fully deployed and does not capture any of the aerodynamic effects of partial deployment. While these data are plotted as a function of Θ, the results are insufficient to make the conclusion that CAA loading can be adequately modeled by this term. As a result, similar simulations were generated at different CAA deployment angles.

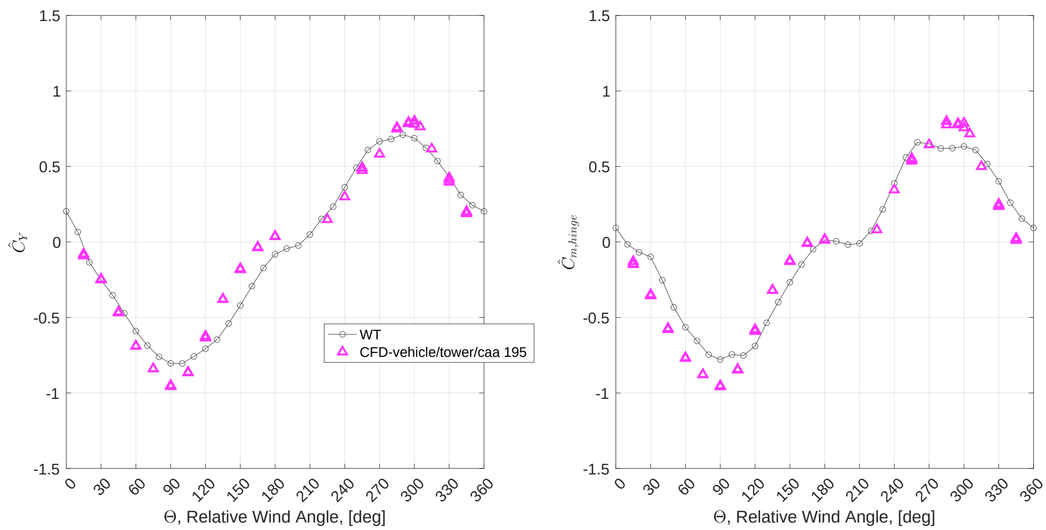

Fig. 8 Normalized side force and hinge moment coefficients on the CAA as a function of relative wind angle comparing WT results to fully deployed CFD cases.

B. Effect of Deployment Angle

Building off the success of Kestrel to compare favorably to the wind tunnel values, it was decided to use it to explore the effect of different deployment angles in addition to ϕ_{azm}. The priority of the points in the run matrix was based on engineering judgment. This selection focused runs to when the CAA was at a γ of 90°, which is about halfway through its motion and minimized the effects of being in proximity of the tower and vehicle. Figure 9 shows the results of these runs at four different deployment angles. The pink triangles are the same fully deployed cases examined earlier, the cyan circles are at a deployment angle of 180°, the blue crosses are the CAA at 150°, and the green diamonds are the CAA at 90°.

When we introduced Θ, it became evident that it would be practical to model $\hat{C}_Y$ and $\hat{C}_{m,hinge}$ as a function of a single variable. The $\gamma = 90°$ cases have higher loading than the fully deployed cases due to the CAA's distance from the ML and vehicle. The shift of the peak from $\Theta = 300°$ to 270° is likely due to the $\gamma = 90°$ cases not being subjected to vehicle and tower proximity effects, which could cause a slight deficit on CAA loading. Overall, this variation shows that the proximity effects of the ML and vehicle do not play a large role in loading outside a few key conditions.

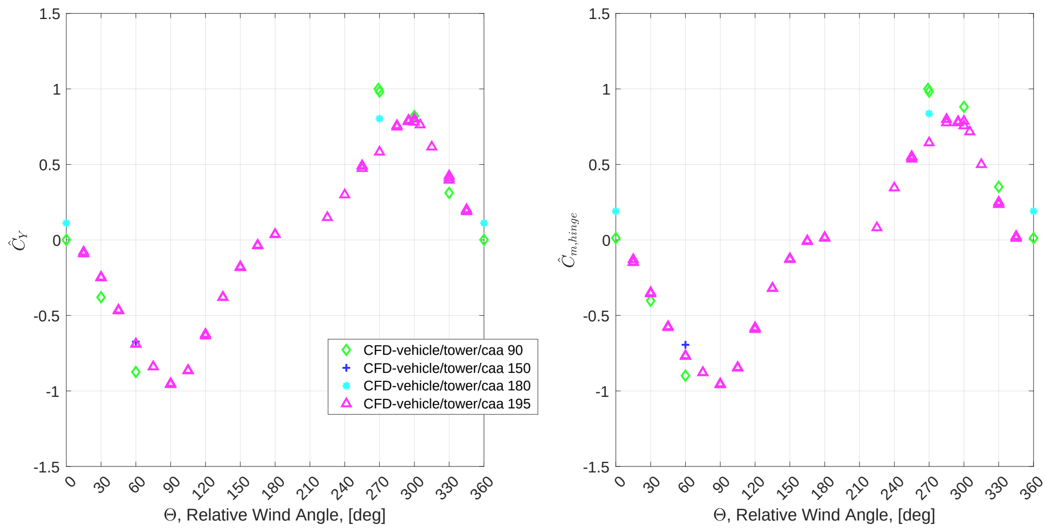

Fig. 9 Normalized side force and hinge moment coefficient on the CAA as a function of relative wind angle comparing CAA at different deployment angles.

C. Isolated CAA

In addition to the previously-discussed analysis, simulations were executed with the isolated CAA. This decision was made such that the deployment with the maximum loads can be determined to decrease the size of the computational run matrix. With the results of the previous section showing that adequate modeling could be done by combining deployment angle and wind angle, it was decided to see if the CAA alone CFD could be used to form the basis of the aerodynamic database.

The results of the CAA alone runs can be found in Fig. 10 in which the isolated CAA cases are compared to the higher-fidelity geometry simulations. Where conditions overlap, the CAA alone cases (the red squares) compare very similarly to the CAA at a deployment angle of 90°. The agreement is greater for $\hat{C}_{m,hinge}$ than $\hat{C}_Y$, which is probably a function of the moment reference point being at the hinge joining the CAA to the tower. The greater agreement in the moment than the force would imply that decreased differences are observed with increasing distance from the tower.

One of the significant differences between the CAA alone and fully deployed is the missing plateau from $\Theta = 180°$ to 210°. The missing plateau is likely due to the exclusion of the tower. Since the primary user of the database is interested in the max loading cases, poor agreement in these data are not a particularly large concern. The disagreement between the peak values at $\Theta = 90°$ is not insignificant, and thus, this difference has been included in a system uncertainty factor in the delivered database. There are significant disagreements in the other forces and moments not shown here, but the database driving this analysis does not capture these other forces and moments and so, are neglected in this analysis. If the requirements of this database change, these other forces and moments would need to be reexamined.

D. Dynamic CAA

To check that the quasisteady state assumptions used in database generation were valid, a single moving case was executed. The results in Fig. 11 show the dynamic CAA in comparison to the rest of the CFD data. The dynamic data shown in a red line start at $\Theta = 270°$, pass through 360°, and ends at 105°. The data are the instantaneous results from the CFD solver and no time averaging or other filtering is applied. The first several thousand time steps are excluded as they include unwanted transients as the flow gets set up.

Of note is that the peak values for both $\hat{C}_Y$ and $\hat{C}_{m,hinge}$ are shifted slightly to the right. This new peak corresponds to the startup portion of the movement. While the peak value in $\hat{C}_Y$ remains about the same, the $\hat{C}_{m,hinge}$ for the dynamic case is about 15% higher than the previously observed maximum value. This makes some intuitive sense because the white room acts as a large "scope" as it moves through space, which would locally increase the loading on the furthest portions of the CAA from the hinge. As the white room acts as a large scoop, an increase in local loading, relative to the static CAA, would be observed at the outboard-most CAA locations. The minimum force and moment

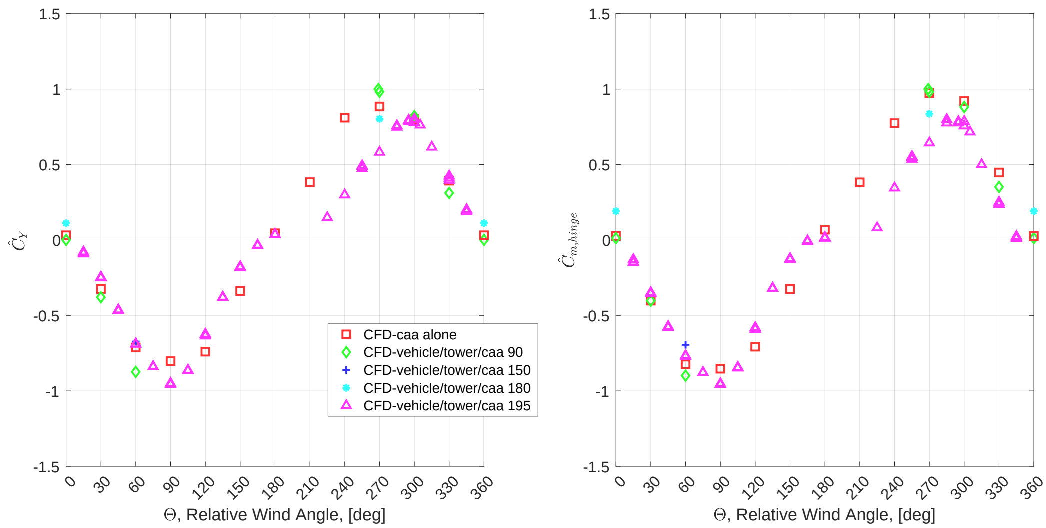

Fig. 10 Normalized side force and hinge moment coefficient on the CAA as a function of relative wind angle comparing CAA near tower and vehicle to isolated CAA.

at Θ = 90° is at the same location as the static cases; however, it is predicted to be closer to zero. Overall, the results of the dynamic case do not raise any concerns about the quasisteady state assumptions used in database generation as the database uncertainty values account for the limitations of the quasisteady state assumption.

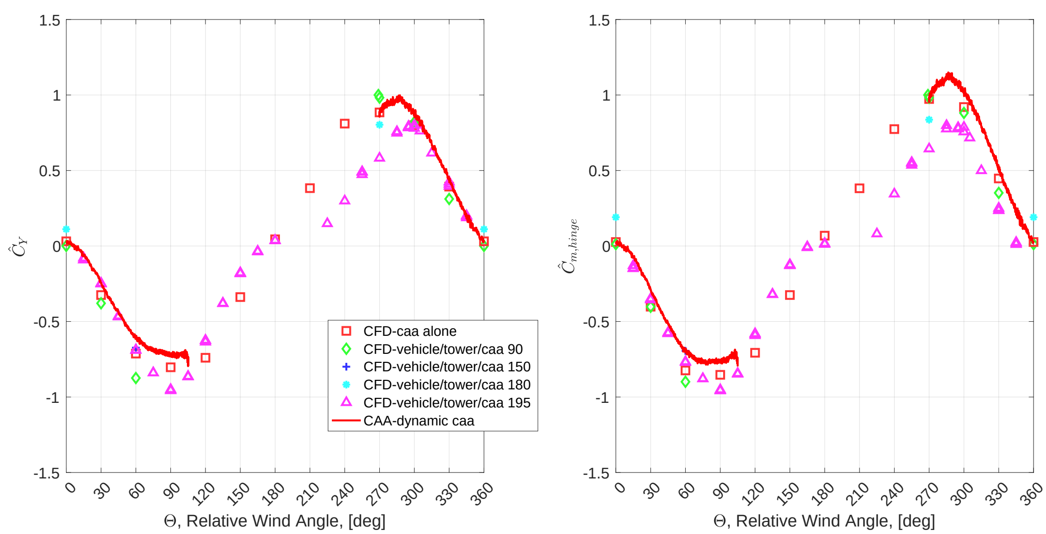

Fig. 11 Normalized side force and hinge moment coefficients on the CAA as a function of relative wind angle comparing stationary CFD cases with the dynamic CAA case.

VI. Conclusion

While building a database to characterize the aerodynamic loading on the CAA, WT and CFD data were compared showing good agreement between them. This agreement led to higher confidence in the ability of both CFD and WT products due to their different approaches to the problem. The limitation of WT hardware in being able to set the CAA at different γ values led to CFD being the primary tool of database delivery. Through the introduction of the relative wind angle, Θ, results from the isolated CAA can be used to characterize the space. While some isolated CAA conditions underpredict $\hat{C}_Y$ relative to data generated with the ML and vehicle, the $\hat{C}_{m,hinge}$ values fall in line with other collected data and as currently designed is the primary metric of interest for the database.

A moving-body CAA case indicates that moving body dynamics play a role in the integrated forces and moments. However, the difference between static and dynamic moments are not considered significant for the database requirements. If a tighter uncertainty quantification is necessary, examination of more dynamic cases is warranted. While a single dynamic run was approximately five times more expensive than the static CAA cases, it does point to the possibility of filling the complete database with two smartly placed runs to cover the full 360° and should be considered if further analysis is necessary.

Overall, this work shows the validity of superposition assumptions in the WT for subcomponents on the ML. By comparing the experimental and computational results, the superposition methodology proved accurate enough that it could have been used if CFD data were not available. Quantification of these differences would necessitate a large computational simulation matrix as well as additional instrumentation in the wind tunnel. The first step would be to minimize the difference in the geometry between the two. As is, the simplifications in detail for both the WT and the CFD were not made to most accurately capture loading on the CAA and so the agreement between the two methods gives greater confidence in both of them.

The 10 times reduction in computational cost of the isolated CAA cases, while usually being more conservative than simulations with the ML and vehicle, points to the continued validity and use of simplifying complex configurations in these analyses. While proximity effects from the tower and vehicle affect loading on the CAA, they tend to cause a reduction in the loading of interest. This conservation in the isolated CAA cases allowed for a significant reduction in computational costs for the database especially when combined with the introduction of Θ.

References

[1] "Crew Access Arm," Available at `https://www.nasa.gov/centers/kennedy/home/orion_crew_access_arm.html`, Accessed: 2022-10-19.

[2] Collins, J. G., Mears, L. J., Shea, P. R., Langston, S. L., Walker, M. A., and Pinier, J. T., "Improved Techniques for Measuring Static Ground Wind Loads on the NASA Space Launch System Mobile Launcher 2," AIAA Paper 2023-XXXX, AIAA SCITECH Forum, National Harbor, MD, 2023.

[3] Pomeroy, B. W., Krist, S. E., Wignall, T., Lee, M. W., Ghaffari, F., Deere, K. A., Collins, J. G., Ratnayake, N. A., Streett, C. L., Goushcha, O. O., Vogel, E. A., and Pinier, J. T., "NASA Langley Low-Speed CFD Contributions to the Space Launch System Program," AIAA Paper 2023-XXXX, AIAA SCITECH Forum, National Harbor, MD, 2023.

[4] McDaniel, D. R., Tuckey, T. R., and Morton, S. A., "The HPCMP CREATE-AV Kestrel Computational Environment and its Relation to NASA's CFD Vision 2030," AIAA Paper 2017-0813, AIAA SciTech Forum, Grapevine, TX, 2017.

[5] McDaniel, D. R., and Tuckey, T. R., "HPCMP CREATE-AV Kestrel New and Emerging Capabilities," AIAA Paper 2020-1525, AIAA SciTech Forum, Orlando, FL, 2020.

[6] Morton, S. A., and Meakin, R. L., "HPCMP CREATE-AV Kestrel Architecture, Capabilities, and Long Term Plan for Fixed-Wing Aircraft Simulations," AIAA Paper 2016-0565, AIAA SciTech Forum, San Diego, CA, 2016.

[7] Morton, S. A., McDaniel, D. R., Sears, D. R., Tillman, B., and Tuckey, T. R., "Kestrel - A Fixed Wing Virtual Aircraft Product of the CREATE Program," AIAA Paper 2009-338, AIAA Aerospace Sciences Meeting, Orlando, FL, 2009.

[8] Pomeroy, B. W., and Krist, S. E., "Validation of Kestrel IDDES Simulations for SLS Transition Analysis," *AIAA Scitech Forum*, 2022.

[9] Ratnayake, N. A., Krist, S. E., Ghaffari, F., and Deere, K. A., "Computational Fluid Dynamics Methods Used in the Development of the Space Launch System Liftoff and Transition Lineloads Databases," *AIAA Aviation Forum*, 2019.

[10] Ratnayake, N. A., Krist, S. E., and Ghaffari, F., "Selection of Computational Fluid Dynamics Tools Used in Development of the Space Launch System Liftoff and Transition Lineloads Databases," AIAA Paper 2019-1840, AIAA SciTech Forum, San Diego, CA, 2019.